Available online at www.sciencedirect.com
SCIENCE DIRECT®
Journal of Solid State Chemistry 177 (2004) 1045–1052
JOURNAL OF SOLID STATE CHEMISTRY
http://elsevier.com/locate/jssc

Mechanisms of molybdenum substitution in vanadium antimonate

Massimo Cimini,[a,b] Jean-Marc M. Millet,[a,*] and Fabrizio Cavani[b]

[a] *Institut de Recherches sur la Catalyse, Chimie CNRS, conventionné avec l'Université Claude-Bernard, Lyon I, 2 av. A. Einstein, 69626 Villeurbanne, France*

[b] *Dipartimento di Chimica industriale e dei Materiali, Viale Risorgimento 4, 40136 Bologna, Italy*

Received 22 July 2003; received in revised form 3 October 2003; accepted 21 October 2003

Abstract

The formation of a solid solution containing the three elements V, Sb and Mo, which are key-elements in the design of light alkane oxidation catalysts, has been studied by incorporating molybdenum into the pure $VSbO_4$ compound as obtained in air at 700°C ($V^{3+}_{0.28}V^{4+}_{0.64}\square_{0.16}Sb^{5+}_{0.92}O_4$). Monophasic compounds with a rutile-type structure have been obtained and characterized by X-ray diffraction, electron microscopy, Infrared Fourier transform, X-ray absorption and electron spin resonance spectroscopies. At low molybdenum content, Mo^{6+} substitute V^{4+} in the cationic-deficient structure. The charge balance is maintained by an increase of the cationic vacancy number. This leads to the formation of a solid solution corresponding to the formula $V^{3+}_{0.28}V^{4+}_{0.64-3x}Mo^{6+}_{2x}\square_{0.16+x}Sb^{5+}_{0.92}O_4$ with $0<x<0.09$. At higher molybdenum content, Mo^{5+} are stabilized and substitute Sb^{5+} in the rutile structure: $V^{3+}_{0.28}V^{4+}_{0.37}Mo^{6+}_{0.18}\square_{0.25}Mo^{5+}_{y}Sb^{5+}_{0.9-y}O_4$ with $0<y<0.06$. At higher molybdenum content the rutile phase is no longer stable and two new phases are formed: Sb_2O_4 and a new mixed vanadium molybdenum antimonate.

Keywords: Rutile-type structure; Vanadium antimonate; Mechanism of substitution; Heterogeneous catalysis; Propane oxidation and ammoxidation catalyst

1. Introduction

Vanadium antimonate-based catalysts are known to be efficient catalysts for the ammoxidation of propane to acrylonitrile. The main phase of these catalysts which include V/Sb/(W,Al)/O [1–4], Fe/V/Sb/O [5,6], Cr/V/Sb/O [7], Sn/V/Sb/O [8], and V/Nb/Sb/O systems [9] is a rutile-type phase. In this phase, the components essential for the activation of propane like V or Fe and those which are active in the NH^{2-}-insertion on the allylic-type intermediate like Sb, are in a close vicinity.

This close vicinity of the different elements in the same structure is thought to be the key to their efficient co-operation in the transformation of the propane; in parallel, an excess of antimony oxide on its surface either in the form of a disperse oxide layer or simply in the form of a surface enrichment in Sb, also plays an important role in the reaction mechanism [7,10,11].

Among the most active and selective propene ammoxidation catalysts, molybdenum is thought to play the role of NH^{2-}-insertion onto the allylic intermediate. This element is also present in a new class of propane ammoxidation catalysts based on V/Mo/Nb/Sb/O mixed oxide [12]. While the active phase of these catalysts has a structure and a composition very different from the rutile-type, the same cooperation between V, Mo and co-elements based on the same principle is observed [13–15].

The goal of this study was to improve the rutile-type catalysts; building on the specific role of Mo, we have attempted to synthesize a rutile-type phase containing V, Mo and Sb cations. The pure vanadium antimonate phase was described as a non-stoichiometric solid solution containing both V^{3+} and V^{4+} and cationic vacancies: $V_{0.9}\square_{0.2-x}Sb_{0.9+x}O_4$ with $0<x<0.2$ [16]. When prepared under air, the compound was reported with the composition $V_{0.92}\square_{0.16}Sb_{0.92}O_4$ [17]. Such a composition was later confirmed by Hansel et al. by neutron and X-ray diffraction [18]. The presence of V^{4+} in this compound had earlier been established by ESR [19]. Several metal cations like W, Al, Cr, Fe, and Ti have already been studied as substituents to vanadium or antimony in these phases [6, 20–23]. W has been

*Corresponding author. Fax: 33(0)472445399.
E-mail address: millet@catalyse.cnrs.fr (J.-M.M. Millet).

0022-4596/$ - see front matter © 2003 Elsevier Inc. All rights reserved.
doi:10.1016/j.jssc.2003.10.010

shown to substitute V in the compound leading to the composition of the type $V_{0.9-x}W_xSbO_4$. Tungsten is proposed to have oxidation state 4+ and substitute V^{4+} whereas the number of cationic vacancies is not affected by the substitution [20]. For Al and Cr what has indeed been studied is the substitution of these elements by V [7,21]. In both cases solid solution of the type $M_{1-x}V_xSbO_4$ with M = Al or Cr and $0<x<0.5$ were observed. In such a composition range no cationic vacancies were reported. For Fe, the entire range of V substitution has been studied [6]. For the Fe rich part of the solid solution the results obtained confirmed those obtained with Al and Cr. In the poor Fe part, Fe was shown to substitute V^{4+}. In such a case the number of cationic vacancies was not affected but anionic vacancies or shear defects involving face-shared octahedra resulting in the same anion deficiency were formed to balance the charge discrepancy. In the case of Ti, two substitution mechanisms were shown to occur in parallel, namely one Ti^{4+} substitutes for one V^{4+} and two Ti^{4+} substitute for one V^{3+} and one Sb^{5+} [22].

In the present work, we report on the crystal chemistry of vanadium antimonate partially substituted by molybdenum. In order to determine the oxidation state of the metallic cations and to understand the mechanism of substitution of vanadium by molybdenum in the synthesized compounds, we have characterized them by chemical analysis, X-ray diffraction, infrared, Xanes and X-ray photoelectron spectroscopies, electron paramagnetic resonance and high-resolution transmission electron microscopy.

2. Experimental

2.1. Synthesis

The molybdenum-containing vanadium antimonates were prepared using a coprecipitation method described elsewhere [23]. It involved the dissolution of vanadium and molybdenum acetylacetonate ($VO(acac)_2$, $MoO_2(acac)_2$) and $SbCl_5$ in absolute ethanol, followed by dropping the solution into a buffered aqueous solution maintained at pH 7. The precipitate obtained was separated from the supernatant liquid by centrifugation and filtration and dried at 120°C all night. The dried solids were heated at a rate of 5°C min^{-1} under air to 340°C for 1 h and to 700°C for 3 h before being quenched. Five compounds with increasing molybdenum content have been prepared. They will be referred from Mo_0, which correspond to the pure vanadium antimonate, to Mo_4.

2.2. Characterization

All synthesized samples have been characterized by several physical techniques. The antimony, molybdenum, and vanadium contents were quantitatively determined by atomic absorption with a precision of about 2%. Powder X-ray diffraction (XRD) patterns were obtained using a BRUKER D5005 diffractometer and Cu$K\alpha$ radiation. They were recorded with 0.02°(2θ) steps over 10–80° angular range with 10 s counting time per step. Sb L_I Xanes spectra were collected at the LURE synchrotron facility in Orsay. They were recorded at 25°C with a varying energy step of 0.9 eV/1 s in the range 4660–4680, 0.3 eV/1 s in the range 4680–4735 and 0.6 eV/1 s in the range 4735–4780, with 3 scans per sample, and using a Si(3,1,1) double crystal. Absorption background carrying out and spectra normalization were made as described elsewhere [24]. $SbPO_4$ and $FeSbO_4$ reference spectra were taken as model data for Sb^{3+} and Sb^{5+}, respectively. EPR spectra have been recorded using a VARIAN E9 spectrometer operating in the X-band mode. DPPH (3314 G, $g = 2.0036$) was used as a standard for g-value determinations. Samples of ca. 30 mg were placed inside a quartz probe cell and analyzed at −196°C. The EPR data were directly fed into a PC computer to be processed as desired. The intensity of the ESR spectra has been measured and compared to that of a standard $VOSO_4$ solution to determine the V^{4+} content of the compounds. When the spectra showed two signals, they were decomposed and the sub-spectra were integrated and calibrated separately [25]. The relative experimental error on the quantitative determination is rather low and standard deviation should be at least equal to 10%. XPS measurements were performed with a VG ESCALAB 200 R. Charging of catalyst samples was corrected by setting the binding energy of adventitious carbon (C1s) at 284.5 eV. Experimental precision on quantitative measurements was considered to be around 10%.

High-resolution electron microscopy was performed with a JEM 2010 ($C_s = 0.5$ mm) equipped with an EDS LINK-ISIS. The accelerating voltage was 200 kV with a LaB_6 emission current, a point resolution of 0.195 nm and a useful limit of information of 0.14 nm. The EDX analyses were conducted using a 25 nm probe size. Standard deviations were evaluated for atomic ratios from 20 analyses. IR spectra were recorded with an FTIR spectrometer (IFS110 BRÜKER) using the KBr pellet technique for sample preparation.

3. Results

3.1. Bulk and surface composition

The results of the chemical analysis of the synthesized compounds are presented in Table 1. It can be seen that for Mo_1 and Mo_2, the (Mo + V)/Sb ratio remained almost constant, which was not the case for the compound with higher molybdenum content. The

Table 1
Composition of the solids calculated from the results of the chemical analysis compared to that calculated from the solid solution formula (7) and (9)

Compound	Composition	
	Experimental	Theoretical
Mo_0	$V_{0.93}Sb_{0.91}O_{4.00}$	$V_{0.92}Sb_{0.92}O_{4.00}$
Mo_1	$Mo_{0.08}V_{0.77}Sb_{0.92}O_{4.00}$	$Mo_{0.09}V_{0.78}Sb_{0.92}O_{4.00}$
Mo_2	$Mo_{0.17}V_{0.73}Sb_{0.95}O_{4.00}$	$Mo_{0.14}V_{0.73}Sb_{0.92}O_{4.00}$
Mo_3	$Mo_{0.22}V_{0.62}Sb_{0.79}O_{4.00}$	$Mo_{0.24}V_{0.65}Sb_{0.86}O_{4.00}$
Mo_4	$Mo_{0.26}V_{0.68}Sb_{0.92}O_{4.00}$	

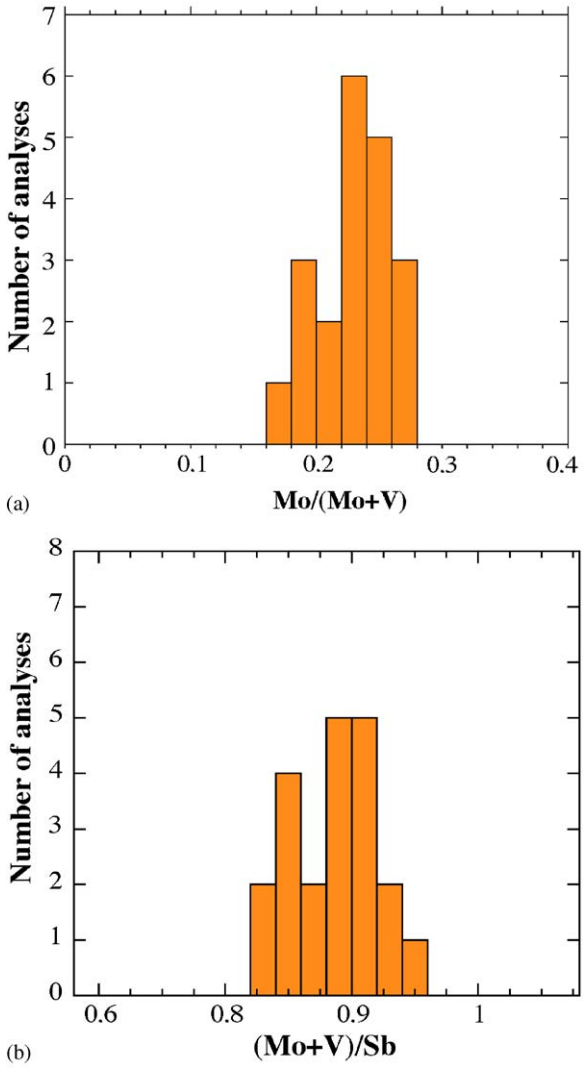

Fig. 1. Histograms of the X-ray microanalysis results of compound Mo_2: (a) Mo/(Mo + V) ratio, and (b) (V + Mo)/Sb ratio.

homogeneity of the composition of solids has been checked by EDX analysis in the course of an electron microscopy study of compound Mo_2. Fig. 1 shows the results obtained describing a narrow compositional population with Mo/(Mo + V) and (Mo + V)/Sb ratios close to those determined by chemical analysis. The surface composition of the solids has been studied by XPS (Table 2). It can be seen that the surface composition is vanadium deficient. The peak energies corresponding to the different metals have been determined (Table 2). They were a characteristic of Sb^{5+}, V^{4+} and Mo^{6+}. The lack of sensibility in vanadium peak determination did not allow the deconvolution of the peak into two peaks that would have corresponded to V^{3+} and V^{4+}. This was not the case of the $Mo3d_{3/2}$ peak in the solid Mo_3, which displayed a shoulder. It has been possible to distinguish two peaks separated by approximately 1 eV, which have been attributed to Mo^{6+} and Mo^{5+} cations. The relative $Mo^{5+}/(Mo^{6+} + Mo^{5+})$ ratio was determined to be around 0.06.

3.2. Phase composition and structure

The X-ray diffraction patterns of the solids are presented in Fig. 2. For Mo_0, Mo_1, Mo_2 and Mo_3, they correspond to a single well-crystallized rutile-type phase. The cell parameters of the simple tetragonal cell have been calculated and are presented in Table 3. Only a slight increase of a and a slight decrease of c were observed with the substitution (Fig. 3). Such a result can be explained by the very close values of the radii of the metallic cations susceptible to be present in the solid solution (V^{3+}: 78 pm, V^{4+}: 72 pm, Sb^{5+}: 74 pm, Mo^{6+}: 73 pm and Mo^{5+}: 75 pm) [26]. The values considered correspond to high-spin cations in 6 coordination. The pattern of the last compound, Mo_4, showed the presence of three phases, the rutile-type phase, Sb_2O_4 and a new phase (Fig. 4).

The electron diffraction pattern of this new phase has been indexed (Fig. 5). The phase crystallizes in the orthorhombic system. The data obtained by electron microscopy made it possible to index the X-ray diffraction powder pattern of the phase mixture and to refine the cell parameters of the phases. The refined cell parameters of the phase are, respectively, equal to

$$a = 0.45412(6)\ \text{nm}, \quad b = 0.5465(1)\ \text{nm}$$
$$\text{and } c = 2.0309(3)\ \text{nm}.$$

X-ray microanalyses gave V/Mo and V/Sb ratios, respectively, equal to 0.52 ± 0.04 and 0.58 ± 0.03 for this new phase. As can be seen in the electron micrograph of the phase, the crystal are large and composed of lamells (Fig. 6). The lamellar character of this phase may also be expected from its X-ray diffraction pattern which exhibits an intense peak at $2\theta = 9.71°$ that may correspond to an interlayer spacing of 1.014 nm. The preparation of this pure phase and the determination of its structure has been undertaken.

Table 2
Binding energies and surface atomic ratios calculated from XPS data on the catalyst

Compounds	Mo3d5/2	Mo3d3/2	V2p3/2	Sb3d5/2	Mo/(Mo+V) (eV)	Sb/(Mo+V)	$Mo^{5+}/(Mo^{5+}+Mo^{6+})$
Mo_0	232.4	235.5	516.7	530.8	—	1.3	—
Mo_1	232.4	235.6	516.7	530.8	0.28	1.8	0
Mo_2	232.5	235.7	516.7	530.9	0.37	1.8	0
Mo_3	232.5	235.5	517.0	530.8	0.41	1.6	0.07
	231.3	234.5					

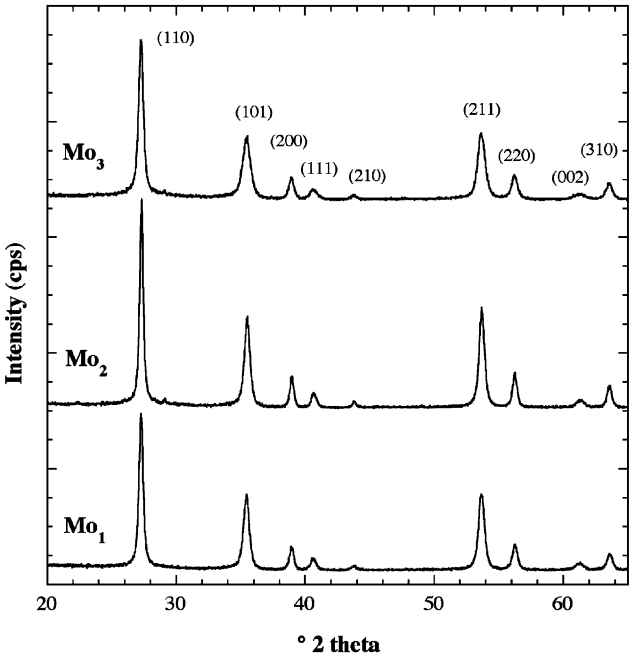

Fig. 2. X-ray diffraction pattern of the Mo containing rutile-type phases.

Table 3
Lattice parameters of the rutile-type phases in the synthesized compounds

Compound	*a* (Å)	*c* (Å)
Mo_0	4.624(1)	3.0332(8)
Mo_1	4.625(1)	3.0270(8)
Mo_2	4.631(1)	3.0261(9)
Mo_3	4.628(1)	3.0248(9)
Mo_4	4.631(6)	3.023(5)

3.3. Oxidation state and stoichiometry

The normalized XANES spectra at the Sb L_1 edge of the studied compounds have been normalized and compared to those of $SbPO_4$ and $FeSbO_4$ which contained, respectively, only Sb^{3+} and Sb^{5+} (Fig. 7). The position of the Sb L_1 edge is sensitive to the oxidation state of antimony. The edge-position of the Sb^{5+} peak is systematically shifted by 4 eV to higher energies with respect to the Sb^{3+} peak, which allows determining the spectrum by fitting the relative amount of the two cations [12,13]. In this case it appeared clearly that the compounds contained only Sb^{5+}.

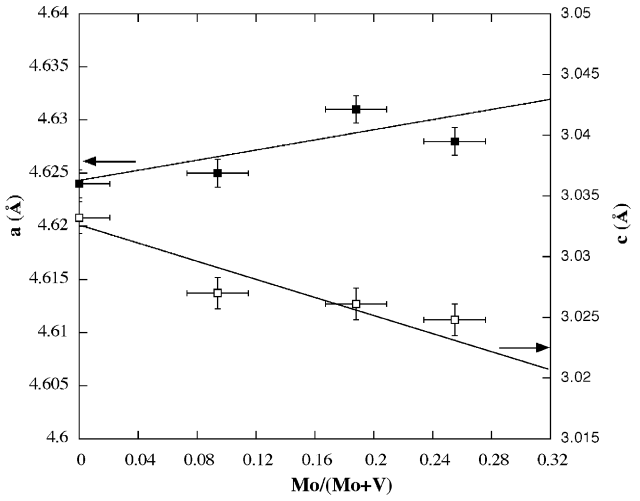

Fig. 3. Cell parameters of the rutile-type compounds: *a* (full circles) and *c* (empty circles) the bars mark the standard deviations taken from EDX and cell parameter calculations.

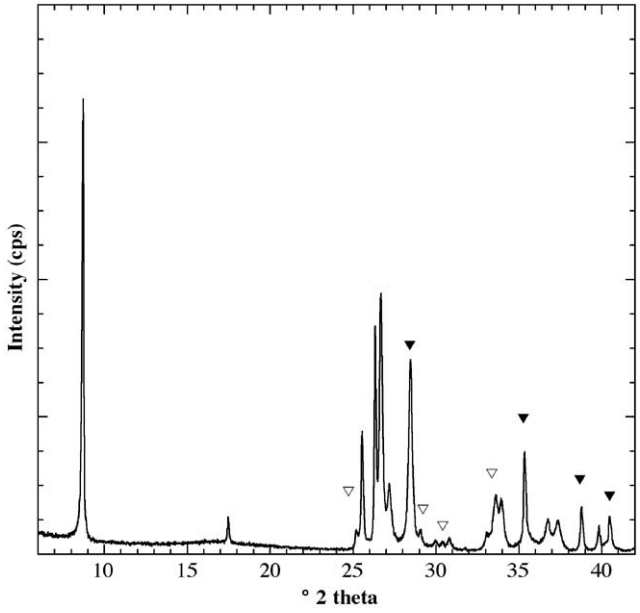

Fig. 4. X-ray diffraction pattern of the sample Mo_4 showing the new phase besides the phase Sb_2O_4 (▽) and the rutile-type phase (▼).

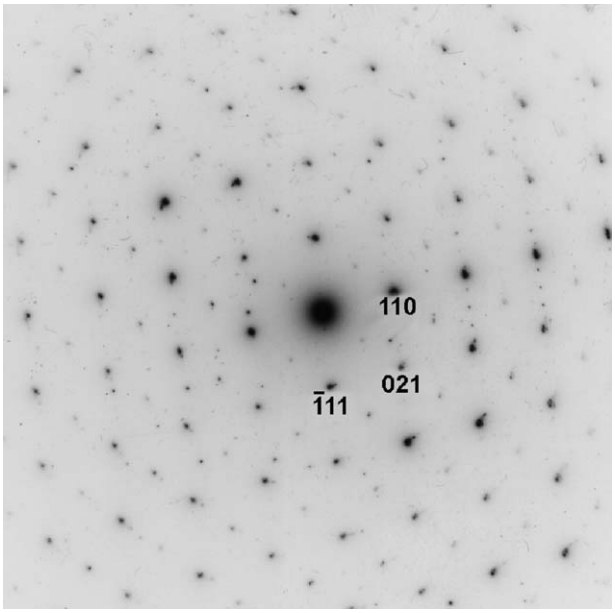

Fig. 5. Indexed electron diffraction pattern of the new phase.

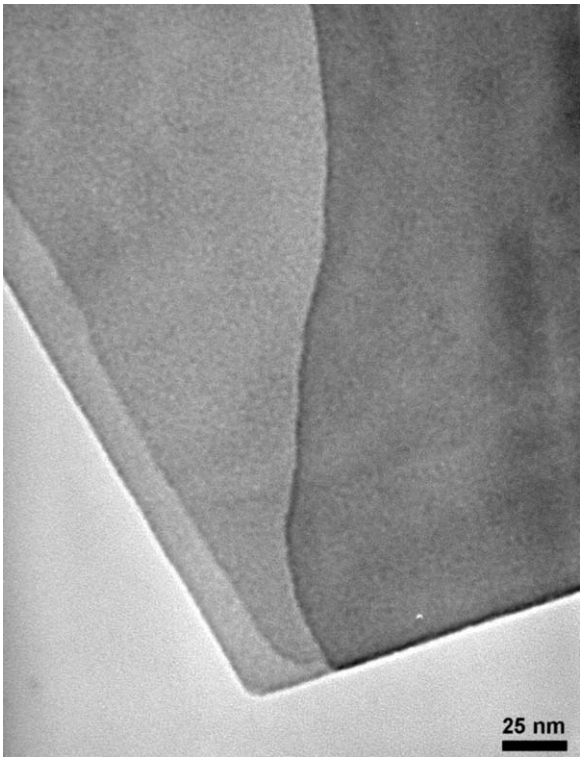

Fig. 6. Transmission electron imaging of the new phase.

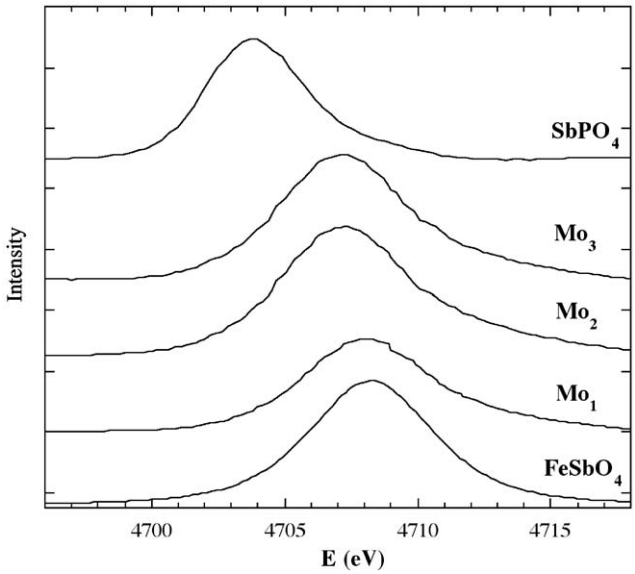

Fig. 7. Normalized XANES spectra at the SbL_1-edge of the rutile-type compounds with those of reference compounds $FeSbO_4$, and $SbPO_4$.

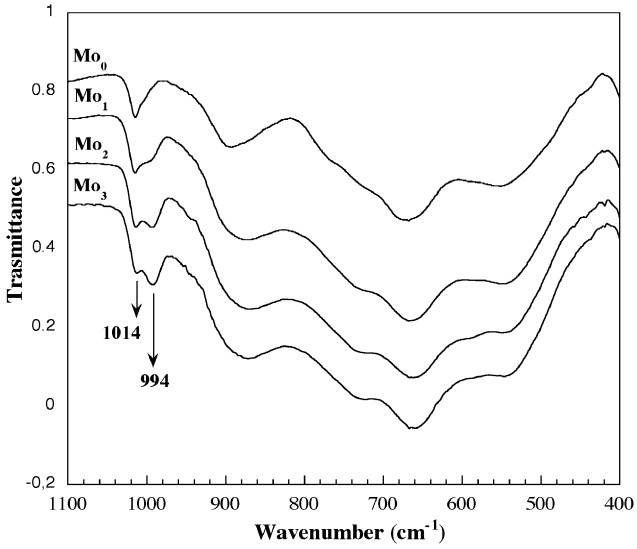

Fig. 8. IR transmission spectra of the Mo substituted rutile-type vanadium antimonates.

Infrared spectra of the prepared compounds are shown in Fig. 8. The bands at 362, 535 and 671 cm^{-1} are typical of the rutile-type structure [14]. Two other bands at 994 and 1015 cm^{-1}, which are present in all the spectra, have, respectively, been attributed to Mo=O vibration and to vibration modes involving the two coordinated oxygen atoms neighboring a cationic vacancy [4]. The intensities of these two bands relative to the band at 535 cm^{-1} have been measured and plotted in Fig. 9 as a function of the Mo content of the solids. It can be seen that the intensity of the band related to Mo=O increases linearly as would have been expected and that of the band taken as proportional to the relative amount of vacancies increases at low Mo content and remains constant at high content (Mo_3).

EPR spectra of the compounds Mo_0, Mo_1, Mo_2 and Mo_3 have been recorded (Fig. 10). The spectra of the three first compounds present two signals. The first one, which represented the majority of the V^{4+} species observable, corresponded to a broad isotropic singlet

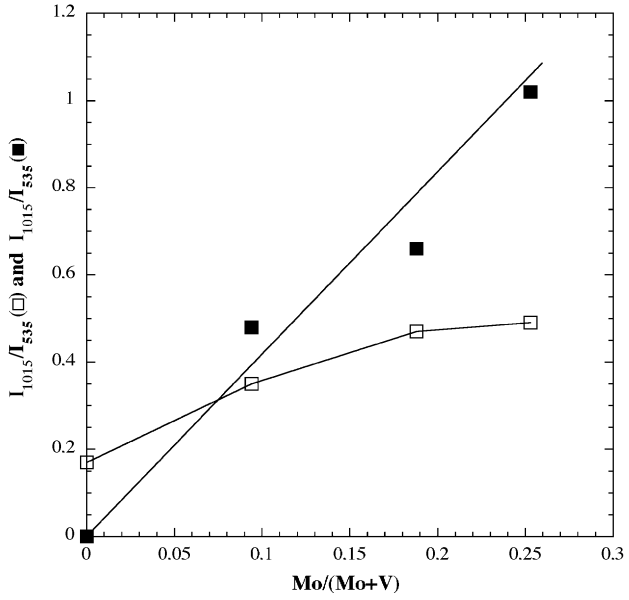

Fig. 9. Intensities of the bands at 994 and 1014 cm^{-1} relative to the band at 535 cm^{-1} as a function of the Mo substitution.

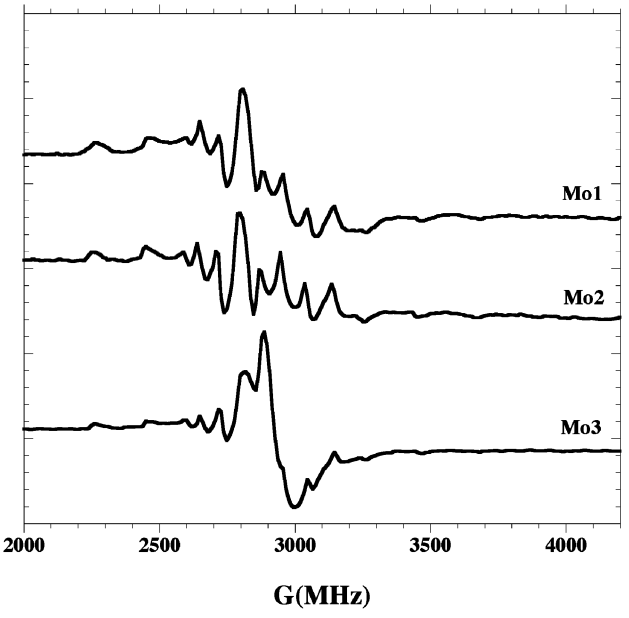

Fig. 10. EPR spectra of the Mo substituted vanadium antimonates with a rutile-type structure.

related to interacting vanadyl species. The second one was a hyperfine signal, which on splitting multiplets, corresponded well to isolated vanadyl species in square pyramidal or distorted octahedral coordination (Table 4). The overall intensity of the ESR spectra and thus the total amount of the observed V^{4+} site decreases with the molybdenum content, which is in good agreement with the substitution of vanadium by molybdenum cations. At the same time the relative intensity of the hyperfine signal increased which could have been predicted

Table 4
g and A parameters of V^{4+} and Mo^{5+} EPR signals in the rutile-type compounds and calculated spin numbers per mg

Compound	species	$g_{\parallel}$	$g_{\perp}$	$A_{\parallel}$(G)	$A_{\perp}$ (G)	spin number[a] (10^{18} mg^{-1})
Mo_0	V(1)	1.934	1.999	202	216	1.500
	V(2)	1.965				
Mo_1	V(1)	1.943	1.966	198	219	1.087
	V(2)	1.950				
Mo_2	V(1)	1.943	1.955	198	214	0.932
	V(2)	1.949				
Mo_3	V(1)	1.943	1.951	198	212	0.500
	V(2)	1.947				
	Mo(1)	1.986	1.900			

[a]The calculated spin number in Mo_3 corresponds only to the vanadium signals.

since molybdenum cations participated in the vanadium site isolation. The spectrum of the Mo_3 was slightly different with a third signal corresponding to Mo^{5+} cations (Fig. 10, Table 4). This signal has been ascribed to Mo^{5+} species. It was characterized by a $g_{\parallel} = 1.986$ and a $g_{\perp} = 1.900$. On the basis of the published data, this signal could be attributed to Mo^{5+} species with an axial symmetry, similar to those reported for Mo^{5+} in the bulk of molybdates [27].

4. Discussion

The detection by electron microscopy of no other phase than the rutile-type phase and the narrow distribution of Mo, V and Sb cations in the particles show that molybdenum is incorporated in the structure and that a solid solution is formed. All the other characterizations tend to confirm this proposition. It is known that substitution of cations in the rutile structure can follow different mechanisms [10]. The substitution of V^{3+} by V^{4+} in $VSbO_4$ when antimonate is prepared under increasing oxygen partial pressures utilizes a substitution mechanism based upon the formation of cationic vacancies according to

$$4V^{3+} \rightleftharpoons 3V^{4+} + \square \quad (1)$$

This leads to the formula for the compounds of the solid solution

$$V^{3+}_{0.9-4x}V^{4+}_{0.2+3x\square x}Sb^{5+}_{0.9}O_4 \quad 0<x<0.2. \quad (2)$$

A second substitution mechanism has been shown to exist for compounds prepared under nitrogen. This mechanism implies a change in the Sb/V ratio and can be expressed as

$$Sb^{5+}+V^{3+} \rightleftharpoons 2V^{4+} \quad (3)$$

The related formula for the compounds of the solid solution is

$$V^{3+}_{0.9-y}V^{4+}_{0.2+2y}Sb^{5+}_{0.9-y}O_4 \quad 0<y<0.7. \tag{4}$$

When heteroatoms are substituted, both types of substitution mechanisms may be encountered. This is the case when tetravalent cations like Ti^{4+} are substituted to vanadium cations [22]. When trivalent cations like Fe^{3+} are substituted again two substitution mechanisms have been proposed [6]. At low substitution level Fe^{3+} substitute V^{4+} and the charge defect is balanced by the formation of anionic vacancies ($\square_O$)

$$O^{2-} + 2V^{4+} \rightleftharpoons 2Fe^{3+} + \square_O \tag{5}$$

In such case the rutile structure with close-packed anion layers should more likely accommodate shear defects involving arrangements of face-shared octahedra than oxygen vacancies resulting however in the same anion deficiency.

At high substitution level the compound no longer contains V^{4+} and Fe^{3+} substitutes V^{3+}

$$V^{3+} \rightleftharpoons Fe^{3+} \tag{6}$$

The oxidation state of molybdenum is higher and both the substitutions of vanadium and antimony were possible. The chemical analyses of the Mo_1 and Mo_2 compounds clearly showed that molybdenum substitutes first preferentially vanadium. ESR results showed a decrease of the total amount of V^{4+} and an increase of the isolated V^{4+} species, in parallel no Mo^{5+} species was detected by this technique. It was obvious that with a heat treatment under air Mo^{6+} would more probably be stabilized. The excess of positive charge brought by the vanadium substitution could either be balanced by a decrease in the oxidation state of antimony or the increase in cationic vacancy number. Xanes spectroscopy clearly showed that antimony remained totally 5+ whereas infrared spectroscopy showed that at the same time the number of cationic vacancies increased as the relative intensity of the band at 1015 cm^{-1} increased. This leads to propose the following substitution mechanism:

$$2Mo^{6+} + \square \rightleftharpoons 3V^{4+} \tag{7}$$

Bringing the oxidation states into the formulas gives for the solid solution compounds

$$V^{3+}_{0.28}V^{4+}_{0.64-3x}Mo^{6+}_{2x}\square_{0.16+x}Sb^{5+}_{0.92}O_4 \text{ with } \quad 0<x<0.09 \tag{8}$$

Such formula explains well the results of chemical analyses and those of EDX on the solid Mo_2. It is interesting to note that the cationic vacancies content (0.25) of the end-member of the solid solution is approximately that of the pure rutile antimonate when heat treated under pure oxygen (0.23) [16]. Such a content may correspond to a limit content for a stable rutile-type structure. The results of the characterization clearly show a different behavior for the Mo_3 compound. The (Mo + V)/Sb is not constant anymore and Mo^{5+} are detected either by ESR or XPS. At the same time the relative amount of cationic vacancies do not increase anymore. This lead to a new mechanism of substitution of the type

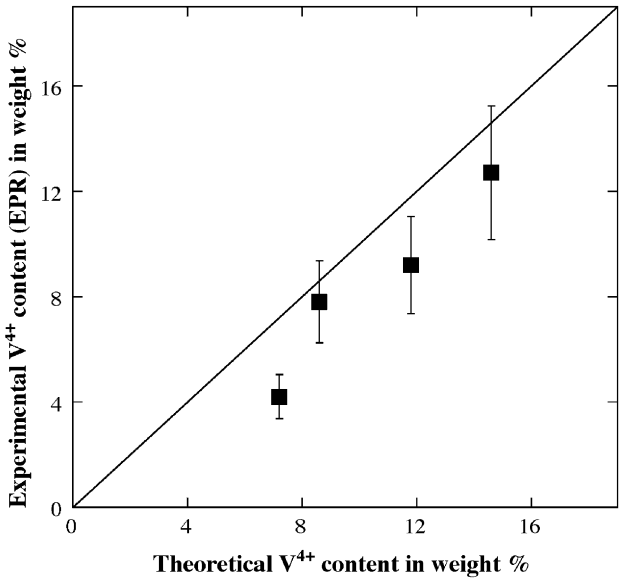

Fig. 11. Experimental V^{4+} content in weight % determined from EPR data as a function of the theoretical V^{4+} content calculated from formula (7) and (9).

$$Mo^{5+} \rightleftharpoons Sb^{5+} \tag{9}$$

with (for the compounds) the formula

$$V^{3+}_{0.28}V^{4+}_{0.37}Mo^{6+}_{0.18}\square_{0.25}Mo^{5+}_{y}Sb^{5+}_{0.92-y}O_4 \text{ with } 0<y<0.06 \tag{10}$$

This second domain of solid solution which is smaller should end for a y value around 0.06 since in the compound Mo_4 with total composition $Mo_{0.26}V_{0.68}Sb_{0.92}O_4$ other phases are detected. Finally, it can be seen in Fig. 11 that the theoretical vanadium content that can be calculated from formula (8) and (10) agrees relatively well with that calculated from EPR results considering spin numbers. At higher Molybdenum content the rutile phase is not stable and a new phase is formed along with Sb_2O_4. This new phase could correspond to that reported by Filipek [28] with the composition $V_2Mo_3Sb_3O_{21}$ although EDX analyses led to a composition slightly different that may evidence the presence of a solid solution.

5. Conclusion

Molybdenum has been shown to partially substitute vanadium in vanadium antimonate with a rutile-type structure. At lower substitution rate, molybdenum cations keep their 6+ oxidation state and substitute

V^{4+} with an increase of the cationic vacancies content for charge balance. Formulas of the type $V^{3+}_{0.28}V^{4+}_{0.64-3x}Mo^{6+}_{2x}\square_{0.16+x}Sb^{5+}_{0.92}O_4$ with x comprised between 0 and approximately 0.09 are obtained for the compounds. At high substitution rate, molybdenum is also present as Mo^{5+} and starts substituting Sb^{5+} leading to formulas of the type $V^{3+}_{0.28}V^{4+}_{0.37}Mo^{6+}_{0.18}\square_{0.25}Mo^{5+}_{y}Sb^{5+}_{0.92-y}O_4$ with y varying from 0 to approximately 0.06. When the molybdenum content is further increased the solid solution is not stable anymore and a mixture of rutile-type phase, Sb_2O_4 and a new phase is obtained.

Acknowledgments

M. Cimini was supported by a Pierre et Marie Curie Scholarship from the European Community.

References

[1] A.T. Guttmann, R.K. Grasselli, J.F. Brazdil, US Patent 4,746,641, 1988, assigned to BP.
[2] G. Centi, R.K. Grasselli, F. Trifirò, Catal. Today 13 (1992) 661.
[3] A. Andersson, S.L.T. Andersson, G. Centi, R.K. Grasselli, M. Sanati, F. Trifirò, Appl. Catal. (A) 113 (1994) 43.
[4] J. Nilsson, A.R. Landa-Canovas, S. Hansen, A. Andersson, J. Catal. 186 (1999) 442.
[5] M. Bowker, C.R. Bicknell, P. Kerwin, Appl. Catal. (A) 136 (1996) 205.
[6] H. Roussel, B. Mehlomakulu, F. Belhadj, E. van Steen, J.M.M. Millet, J. Catal. 205 (2002) 97.
[7] N. Ballarini, F. Cavani, C. Giunchi, S. Masetti, F. Trifirò, D. Ghisletti, U. Cornaro, R. Catani, Topics Catal. 15 (2001) 111.
[8] S. Albonetti, G. Blanchard, P. Burattin, F. Cavani, S. Masetti, F. Trifirò, Catal. Today 42 (1998) 283.
[9] Y. Mimura, K. Ohyachi, I. Matsuura, in: H. Hattori, K. Otsuka (Eds.), Sci. Tech. Catal. 1998, Kodansha, Tokyo, 1999, p. 69.
[10] N. Ballarini, F. Cavani, D. Ghisletti, R. Catani, U. Cornaro, Catal. Today 78 (2003) 273.
[11] F.J. Berry, J.G. Holden, M.H. Loretto, J. Chem. Soc., Dalton Trans. 1727 (1987).
[12] K. Ushikubo, A. Oshima, M. Kayou, M. Vaarkamp, Hatano, J. Catal. 169 (1997) 394.
[13] T. Ushikubo, K. Oshima, T. Ihara, H. Amatsu, US Patent 5,534,650 (1996), assigned to Mitsubishi chemical Co.
[14] J.M.M. Millet, H. Roussel, A. Pigamo, J.L. Dubois, J.C. Jumas, Appl. Catal. (A) 232 (2002) 77.
[15] E.K. Novakova, J.C. Védrine, E.G. Derouane, J. Catal. 211 (2002) 226.
[16] A. LandaCanovas, J. Nilsson, S. Hansen, K. Stahl, A. Andersson, J. Solid State Chem. 116 (1995) 369.
[17] T. Birchall, A.W. Sleight, Inorg. Chem. 15 (1976) 868.
[18] S. Hansen, K. Stahl, R. Nilsson, A. Andersson, J. Solid State Chem. 102 (1993) 340.
[19] F.J. Berry, M.E. Brett, Inorg. Chim. Acta 76 (1983) L205.
[20] J. Nilsson, A.R. Landa-Canovas, S. Hansen, A. Andersson, J. Catal. 186 (1999) 442.
[21] J. Nilsson, A.R. Landa-Canovas, S. Hansen, A. Andersson, J. Catal. 160 (1996) 244.
[22] A. Wickman, L.R. wallenberg, A. Andersson, J. Catal. 194 (2000) 153.
[23] G. Blanchard, P. Burattin, F. Cavani, S. Masetti, F. Trifirò, WO Patent 97/23,287 A1 (1997), assigned to Rhodia.
[24] J.M.M. Millet, E. Baca, A. Pigamo, D. Vitry, W. Ueda, J.L. Dubois, Appl. Catal. (A) 244 (2) (2003) 359.
[25] D.L. Nguyen, Y. Ben Taarit, J.M.M. Millet, Catal. Lett. 90 (1–2) (2003) 65.
[26] R.D. Shannon, C.T. Prewitt, Acta Crystallogr. B 25 (1969) 295.
[27] E. Giamello, F. Theobald, C. Naccache, J.C. Vedrine, J. Chim Phys. 75 (3) (1978) 305.
[28] E. Filipek, J. Therm. Anal. Cal. 64 (2001) 1095.